IMPROVED TESTS OF MUON AND ELECTRON NUMBER CONSERVATION IN MUON PROCESSES

William R. Molzon*
Department of Physics and Astronomy
University of California, Irvine, CA 92697-4575

ABSTRACT

I review the motivation for and status of searches for violation of muon and electron number conservation, concentrating on muon-initiated processes. I discuss the expected progress in these searches and describe a new experiment, E940 at Brookhaven National Laboratory (BNL), recently proposed by the **M**uon to **E**lectron **Co**nversion (MECO) Collaboration and now approved. It will improve the experimental sensitivity for the process $\mu^- N \to e^- N$ to below 10^{-16}, roughly four orders of magnitude better than the current limit.

*Supported by DOE Grant DE-FG03-91ER40679.

1 Introduction

Since the discovery of the muon and the realization that all differences between muons and electrons are attributable solely to the difference in their masses, there has been interest in understanding why more than one *family* of leptons exists and how they are related.

The fact that the decay of a muon to an electron and a photon does not occur led to speculation that both neutrinos and charged leptons carry a quantum number that is at least approximately conserved, and hence that there exists more than one type of neutrino. If this were not the case, this decay would occur through a loop diagram containing a neutrino and a W boson. We now know that only three families of light leptons exist, and that an additive quantum number associated with each family is conserved to a high degree.

One of the fundamental issues in particle physics that remains is an understanding of the pattern of fermions's masses and the closely related issue of flavor mixing, transitions between families of fermions. The latter will occur naturally if the quark and lepton mass eigenstates are not eigenstates of all forces. This is the case for quarks, and the mixing is described by the CKM matrix, which specifies the coupling of a linear combination of the charge 2/3 quarks to a linear combination of the charge –1/3 quarks through the W boson. We know from experimentation that the mass eigenstates are not weak interaction eigenstates, and both the values of the masses of the eigenstates and the mixing of these states via the weak interaction are parameters determined by experimentation. Within this framework, flavor-changing transitions occur, for example, the decay $b \to s\gamma$ as shown in Fig. 1.

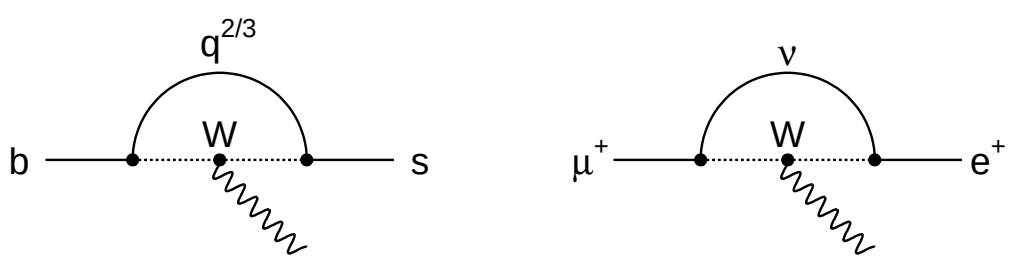

Fig. 1. Feynman diagrams for the process $b \to s\gamma$ and $\mu^+ \to e^+\gamma$ involving a loop containing a W boson and either a charge 2/3 quark or a neutrino.

In the case of leptons, a similar process may occur if neutrinos are not degenerate in mass. In this case, there will be a mixing matrix which relates the mass eigenstates to the weak interaction eigenstates. This could give rise to lepton flavor violating (LFV) interactions, for example, the process $\mu^+ \to e^+\gamma$ as shown in Fig. 1. The same underlying physics will also result in neutrino oscillations, and a great deal of experimental and theoretical effort is devoted to exploring this possibility. Our knowledge of the allowed range of neutrino mass differences and mixing angles precludes the possibility that experimentally observable LFV effects occur via this mechanism.

The fact that neutrino mixing does not lead to lepton flavor violation at observable levels means the discovery of LFV processes would indicate the existence of new physics processes. Searches for such processes are among the most sensitive means at our disposal for looking for physics beyond the Standard Model. They began with the discovery of the muon and are still being done.

There has been recent progress in LFV searches using both kaon and muon processes. We list in Table 1 the LFV processes which have been studied, the current experimental limits on these processes, and their classification in terms of a *generation number* in the model of Cahn and Harari.[1] This model presumes that the process occurs at tree level or in a one-loop diagram, and infers a mass (or mass difference) limit based on the assumption that the coupling strength is that of the electroweak force.

Table 1. LFV violating process, the change in generation number in the model of Cahn and Harari,[1] the current experimental limits, and the inferred limits on intermediate particle masses (updated from the reference for new experimental results).

Process	ΔG	limit	mass limit (TeV)
$K_L^0 \to \mu e$ (Refs. 2, 3)	0,2	2.4×10^{-11}	100
$K_L^0 \to \pi\mu e$ (Ref. 4)	0,2	3.2×10^{-10}	37
$K^+ \to \pi\mu e$ (Ref. 5)	0	2.1×10^{-10}	29
$\mu^+ \to e^+e^+e^-$ (Ref. 6)	1	1.0×10^{-12}	86
$\mu^+ \to e^+\gamma$ (Ref. 7)	1	3.8×10^{-11}	20
$\mu^- N \to e^- N$ (Ref. 8)	1	7.8×10^{-13}	500

There are also limits on lepton flavor violating processes involving the τ lepton ($\tau \to \mu\gamma$) and B meson decays ($B \to \mu e$). The sensitivity is limited by the number of produced τ leptons and B mesons. In both cases, they are not competitive with experiments using muons and kaons, except in restricted models in which, for example, τ decay proceeds by a loop diagram involving Standard Model neutrinos, and the mixing of ν_τ and ν_μ or ν_e is significantly larger than the mixing of ν_μ and ν_e. However, as we have already seen, this possibility is already constrained by other experiments to be well below what is experimentally accessible.

Unlike other conservation laws, electric charge for example, conservation of muon and electron number does not follow from invariance under a local gauge transformation. Hence, there is strong theoretical prejudice that violations will be seen. The discovery of LFV processes would indicate the existence of either a new force mediated by a new gauge boson with nondiagonal lepton couplings or a new class of heavy particles with lepton flavor mixing in this new sector (e.g., supersymmetry). The possibility of LFV exists in essentially all extensions to the Standard Model, and we will discuss some of these in a following section.

In the remainder of this paper, we will briefly discuss physics models which allow lepton flavor violation and the range in parameter space in these models which can be probed by proposed experiments. We will then give an overview of the experimental techniques involved in $\mu \to e^+\gamma$ and $\mu^- N \to e^- N$ experiments, and discuss the experiments which have given the most stringent limits. Finally, we will describe a new experiment which is proposed to improve very substantially the experimental search for $\mu^- N \to e^- N$.

2 Theoretical Motivation for LFV Searches

Aside from the underlying motivation to test conservation laws with the best possible sensitivity, there is theoretical motivation derived from the many proposed extensions to the Standard Model which allow lepton flavor violation. In general, these models are not devised for the purpose of predicting LFV. In many cases, the stringent LFV limits already set restrict the allowed values of parameters within these models. A comprehensive review of the relevant models is beyond the scope of this paper.

Feynman diagrams for new processes which could contribute to LFV are shown in Fig. 2. Among the possibilities are four fermion contact interactions which cou-

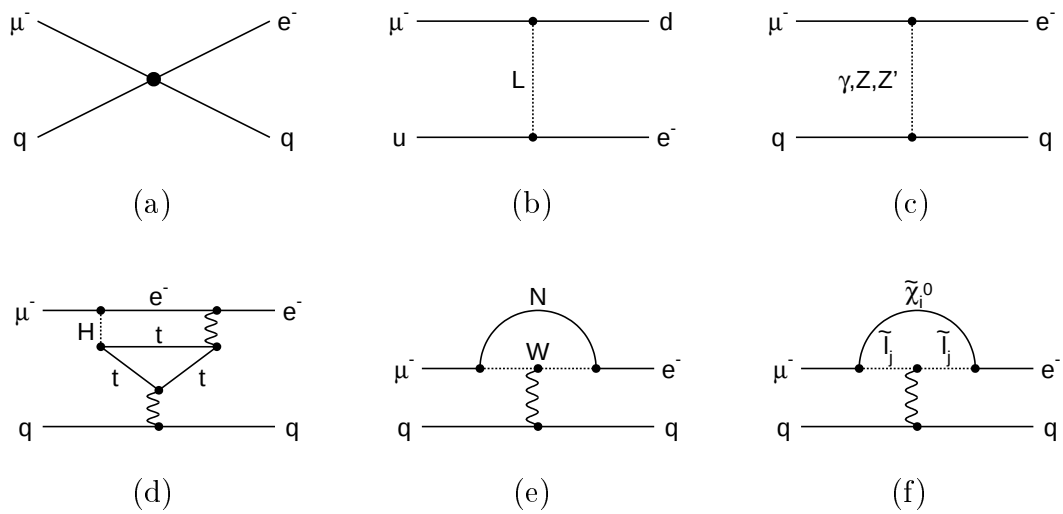

Fig. 2. Feynman diagrams for the process $\mu^- N \to e^- N$ in different scenarios for non-Standard Model physics.

ple quarks and leptons, lepto-quarks with nondiagonal couplings, new Z' gauge bosons which couple nondiagonally to leptons, nondiagonal couplings of Higgs bosons, heavy neutrinos which mix with the known neutrinos, supersymmetry models in which LFV occurs in the supersymmetric sector, horizontal gauge bosons which explicitly couple one lepton family to another, etc.[9] In most models, there is no particular scale at which lepton flavor violation should occur, since masses, coupling strengths, and mixing angles of new particles are not predicted. Nonetheless, the reach in parameter space of current and proposed experiments is impressive. For example, in the case of technicolor, the expectation was that lepton flavor violation would occur at levels which are already ruled out, and these models are severely restricted by limits on LFV. Limits on $\mu^- N \to e^- N$ already require $B(Z^0 \to \mu e) < 10^{-13}$, well below what can be measured by direct detection of that decay.

Much interest has occurred recently in supersymmetric models, in particular in grand unified supersymmetric models. These are particularly attractive, as supersymmetry is perhaps the most realistic candidate to solve many of the shortcomings of the Standard Model. It was realized, first by Hall and Barbieri, that LFV will occur at experimentally accessible levels in a large class of supersymmetric models.[10–13] Further, in some specific grand unified supersymmetric models, the rate for LFV processes can be related directly to Standard Model parameters.

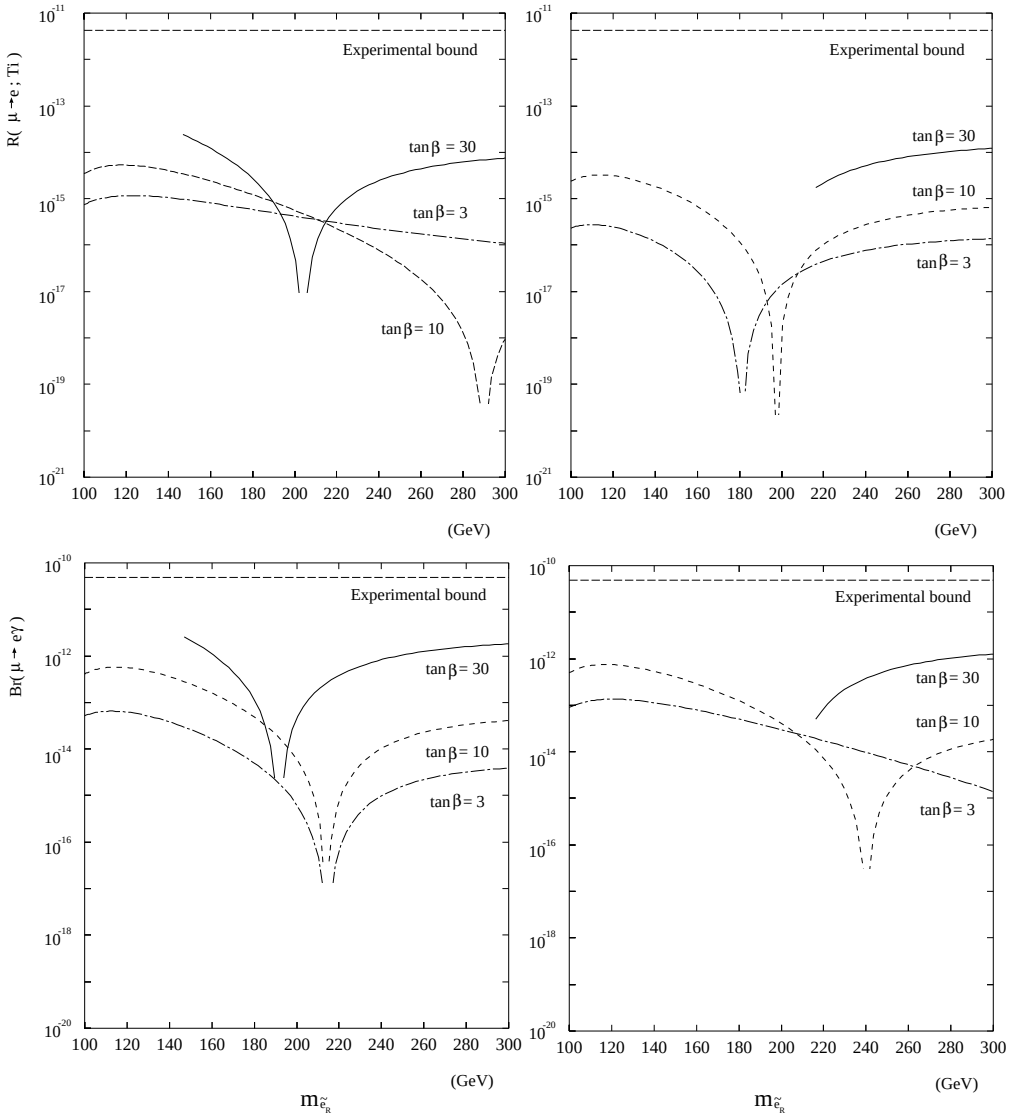

Fig. 3. Expected rates for $\mu^- N \to e^- N$ and $\mu^+ \to e^+\gamma$ in the model of Hisano *et al.* for different values of the ratio of Higgs particle vacuum expectation values as a function of the right-handed selectron mass. The plots are shown for the parameter $\mu > 0$ (left) and $\mu < 0$ (right). The $\mu^- N \to e^- N$ experimental bound has improved to 7.8×10^{-13} since this publication.

The predicted rates for the processes $\mu^- N \to e^- N$ and $\mu^+ \to e^+\gamma$ are plotted in Fig. 3 for one such model.[13] If grand unified supersymmetric models are correct, a search for $\mu^- N \to e^- N$ with sensitivity 10^{-16} or $\mu^+ \to e^+\gamma$ with sensitivity 10^{-14} have a real potential for discovering lepton flavor violation. Even if supersymmetry is discovered by direct observation of new particles, the measurement of LFV violating processes will be extremely important in understanding symmetry breaking in the interactions.

3 Overview of LFV Searches Using Muons

Of the muon-initiated LFV processes, the most familiar is $\mu^+ \to e^+\gamma$ decay. This process has been studied extensively, and the sensitivity of searches continues to improve. There is an ongoing experiment[7] and there have been discussions about the possibility of executing experiments with even better sensitivity.[14] A second process is $\mu \to eee$; it is closely related to $\mu^+ \to e^+\gamma$ if mediated by a γ. If so, at the same branching fraction it is less sensitive to the underlying physics due to an extra factor of α in the decay rate. The limit is already very good,[6] and there are no proposals to do another experiment. A third reaction is $\mu^- N \to e^- N$; it is also closely related to $\mu^+ \to e^+\gamma$ if mediated by a photon. In this case, for the same underlying physics, the ratio $\mathrm{R}_{\mu e} \equiv \Gamma(\mu^- N \to e^- N)/\Gamma(\mu^- N \to \nu N')$ is about 300 times smaller[15] than the branching fraction for $\mu^+ \to e^+\gamma$. There is an ongoing experiment[8] to improve the sensitivity, and a new experiment[16] has been approved to improve it even further.

3.1 Ongoing $\mu^+ \to e^+\gamma$ Experiments

Searches for $\mu^+ \to e^+\gamma$ are conceptually very simple. The signature is a photon and an electron, each with energy $\sim m_\mu/2$, originating from a common point and with opposite momenta. The experiment is performed by bringing a large flux of μ^+ to rest in a thin target and measuring the kinematic properties of the e^+ and γ from the decay.

The principal experimental difficulty lies in distinguishing radiative muon decay from the signal. This intrinsic background arises when both neutrinos are emitted with approximately zero energy, and the final state is indistinguishable from that of the signal. It is reduced by requiring the measured e^+ and γ mo-

menta to be opposite in direction and sufficiently close to $m_\mu/2$ that the radiative decay background satisfying these requirements is below the desired sensitivity. A second source of background arises from the accidental overlap of two decays, one providing the γ and the second providing the e^+. The time and spatial coincidence of the particles' origin provide additional background rejection tools. At the stopping intensities required to measure branching fractions below 10^{-12}, the accidental background dominates.

The state of the art is the MEGA experiment[7] at the Los Alamos Meson Physics Facility (LAMPF). That experiment completed data taking in 1995, and is currently analyzing it. The total exposure consisted of approximately 1.5×10^{14} stopped muons, and about 5×10^8 events written to tape. Briefly, the detector consists of a set of proportional wire chambers, drift chambers, and scintillation counters in a solenoid. The helical trajectory of electrons is measured in drift chambers. Photons are converted in thin radiators and the trajectories of the resulting e^+e^- pairs measured to deduce the photon momentum.

Results of based on $\sim 16\%$ of the data have been reported;[7] from these data an upper limit $\mathrm{B}(\mu^+ \to e^+\gamma) < 3.8 \times 10^{-11}$ at 90% confidence level was set. Based on full analysis of the data and possible improvements in analysis efficiency, an upper limit of 3—6 $\times 10^{-12}$ is expected to be set, assuming no events are seen.

There are no proposals for more sensitive searches for this process, although a number of ideas for experiments which could reach a sensitivity close to 10^{-14} have been discussed.[14]

3.2 Ongoing $\mu^- N \to e^- N$ Experiments

As discussed above, the process $\mu^- N \to e^- N$ is closely related to $\mu^+ \to e^+\gamma$. In one class of models, $\mathrm{R}_{\mu e}$ is ~ 300 times smaller than $\mathrm{B}(\mu^+ \to e\gamma)$ and the sensitivity goals are correspondingly more ambitious. Better sensitivity is possible due to the lack of the kind of accidental backgrounds which limit $\mu^+ \to e^+\gamma$ experiments.

The experiment is done by bringing a large flux of μ^- to rest in a thin target. The μ^- quickly become Coulomb bound to nuclei, and either decay or are captured on the nucleus. For moderate size nuclei, these processes happen at about the same rate, and μ^-'s disappear with a lifetime of about 1 μs. If they convert to electrons, the signature is an isolated electron originating in the stopping target.

There is a large coherent component to the process, proportional to the square of the elastic form factor at 100 MeV/c momentum transfer. This component is large, since the energy transfer to a single nucleon is only 5 MeV. The coherent rate is enhanced by about a factor of Z compared to the rate for muon capture.

The principal experimental difficulties are getting sufficient μ^- flux and reducing backgrounds due to other sources of 105 MeV electrons. One class of backgrounds is intrinsic, resulting from decays of μ^- stopped in matter; they can be reduced only by improved electron energy resolution. A second class results from electron and pion contamination in the beam and from cosmic rays, and these can be reduced or eliminated with beam and detector design. Because there is no inherent accidental background, the stopping rate can be very high. There may, of course, be backgrounds which are sensitive to rate, for example, those due to energy mismeasurement from pileup.

The state of the art is the SINDRUM2 experiment[8] at the Paul Scherrer Institüt (PSI). The first phase is complete, and a limit $R_{\mu e} < 7.8 \times 10^{-13}$ at 90% confidence level has been set. They propose to improve their sensitivity to 4×10^{-14} with a new beam and new background rejection technique. Figure 4 shows a cut view of the apparatus. It is a cylindrical detector, with drift chambers in a solenoid field to measure the e^- momentum. About 10^7 μ^-/s are stopped in a target on the axis of the solenoid. The beam is continuous, and contains a mixture of μ^-'s, π^-'s, and e^-'s. Backgrounds from beam contamination are eliminated by rejecting events in which there is a signal in a thin scintillator in the beam, time coincident with the detected electron. Figure 4 shows the effect of two sets of cuts on the energy spectrum of electrons. After all cuts are applied, beam and cosmic ray induced backgrounds are eliminated, and the intrinsic background due to μ decay in the Coulomb bound orbit is well separated from the signal region.

To further improve the sensitivity, the SINDRUM2 Collaboration has upgraded the μ^- beam to eliminate all π^- and high momentum e^- from the beam. This allows them to remove the beam veto and increase the stopping rate to 10^8 s^{-1}. The beam they propose must reduce π^- and e^- contamination in the beam by a factor of 4000. They are currently taking data with a gold target, and will take data later in 1998 with a titanium target, with a goal of reaching a sensitivity below 10^{-13}.

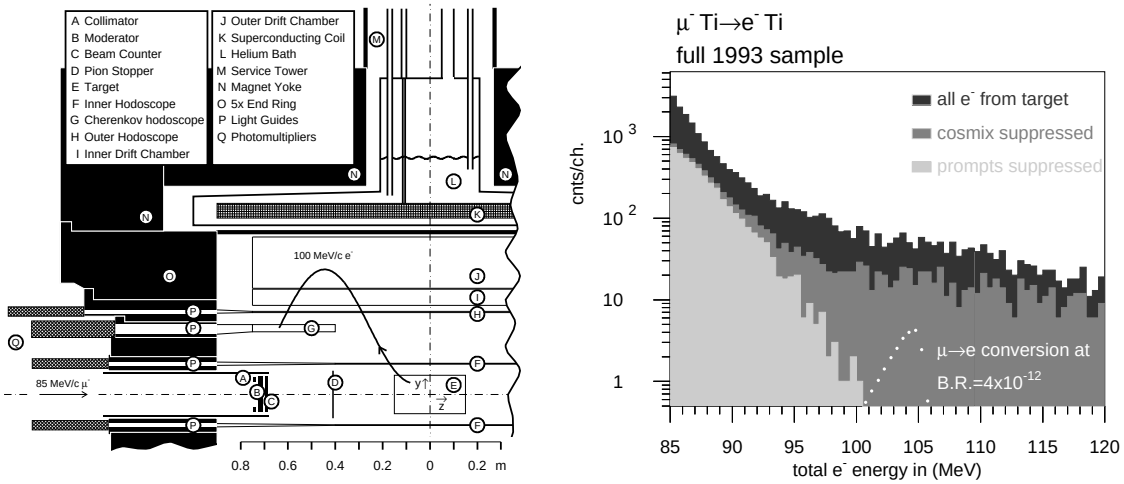

Fig. 4. A cut view of the SINDRUM2 $\mu^- N \rightarrow e^- N$ apparatus is shown on the left. The histogram shows detected electron energy distributions; the lightly shaded contribution is after all cuts have been applied and consists primarily of electrons from muon decay in orbit. The medium shaded region contains background removed by vetoing on events which are in time with a signal in the beam counter, and the heavily shaded area contains events removed by cosmic ray cuts.

Reaching a sensitivity below 10^{-16}, which is the goal of the **M**uon to **E**lectron **Co**nversion (MECO) experiment, will require a much more intense μ^- beam and significantly improved background rejection. It is unlikely that the SINDRUM2 approach can be used.

4 The MECO $\mu^- N \rightarrow e^- N$ Experiment

The MECO Collaboration has recently proposed[16] to extend the experimental sensitivity for $\mu^- N \rightarrow e^- N$ to below 10^{-16} using a new beam and detector operating at the Brookhaven National Laboratory (BNL) Alternating Gradient Synchrotron (AGS).

One critical aspect of MECO is a very intense μ^- beam. The proposed design uses the idea of Djilkibaev and Lobashev[17,18] to place the π production target in a graded solenoidal field and collect π's over an essentially 4π solid angle. They calculated that it should be possible to produce up to $\sim 10^{-4}$ μ^- per proton with this design implemented at a high flux, 600 MeV proton accelerator, the

Moscow Meson Factory (MMF). Due to circumstances beyond the control of the proponents, this machine will not be able to operate enough to execute a sensitive experiment.

The BNL AGS has significantly lower current than that proposed for the MMF, but has higher energy, which is particularly advantageous in producing μ^- beams. The AGS now accelerates 6×10^{13} protons with a 50% duty cycle, three second rep rate, and eight bunches in a 2.7 μs revolution time. AGS accelerator physicists[19] have devised a method of machine operation using only two bunches, with up to 2×10^{13} protons per bunch (4×10^{13} protons per pulse) with 50% duty factor and one second rep rate. Approximately 0.01 μ^- per proton can be produced at the AGS. With even more aggressive muon beam design, in excess of 0.1 μ^- per proton is proposed for the front end of the muon collider.[20,21]

A second critical aspect of MECO is the use of a pulsed beam to reduce significantly the prompt backgrounds from π^- and e^- contamination in the beam. Pulsed beams have been used previously in conversion experiments.[22] The basic idea is to produce a pulsed μ^- beam, stop the muons, and then detect conversion electrons only after all π^- and e^- in the beam have either decayed or passed through the detector region. The spacing between pulses must be sufficient to allow all beam particles to disappear and must be comparable to the μ^- lifetime in the stopping target. These considerations lead to a beam pulse frequency of $\sim$ 1 MHz and the use of an aluminum stopping target, in which the μ^- lifetime is 880 ns. The extinction (ratio of the number of protons between pulses to that in the pulses) has been shown to be required to be about 10^{-10}, in order to reduce background to negligible levels.

A third critical requirement is a detector system capable of measuring e^- momenta with high precision, in order to minimize intrinsic backgrounds. It must be able to operate in the high rate environment resulting from the high μ^- stopping rate.

A schematic drawing of the MECO beam line and experimental area is shown in Fig. 5. Pions are produced from a tungsten target in a solenoid; the axial component of the field is graded, decreasing in the direction of the muon beam. The graded field results in a very high capture probability for π's and μ's, since charged particles emitted away from the μ^- beam direction are reflected, as in a magnetic bottle. The μ^- beam resulting from π^- decays is transported to the stopping target and detector region in a curved transport solenoid. The effect

of the curvature on particles propagating in helical trajectories in the solenoid is exploited to sign- and momentum-select the beam. This is important for rate and background issues, as will be discussed. The region of the production target, transport, and detector are in vacuum.

The μ^- stopping target and detector are located in a detector solenoid, in which the axial component of the field decreases from 2 T at the entrance to 1 T just after the target. The target consists of 17 disks of aluminum, with radius $\sim$ 6 cm and thickness 200 μm. The detector is located downstream of the target in order to minimize rates in it due to particles coming from the target. The use of an axially graded field results in very good acceptance for 105 MeV electrons originating in the target, and allows electrons produced in the upstream pole piece of the production solenoid to be unambiguously distinguished from those produced in the target.

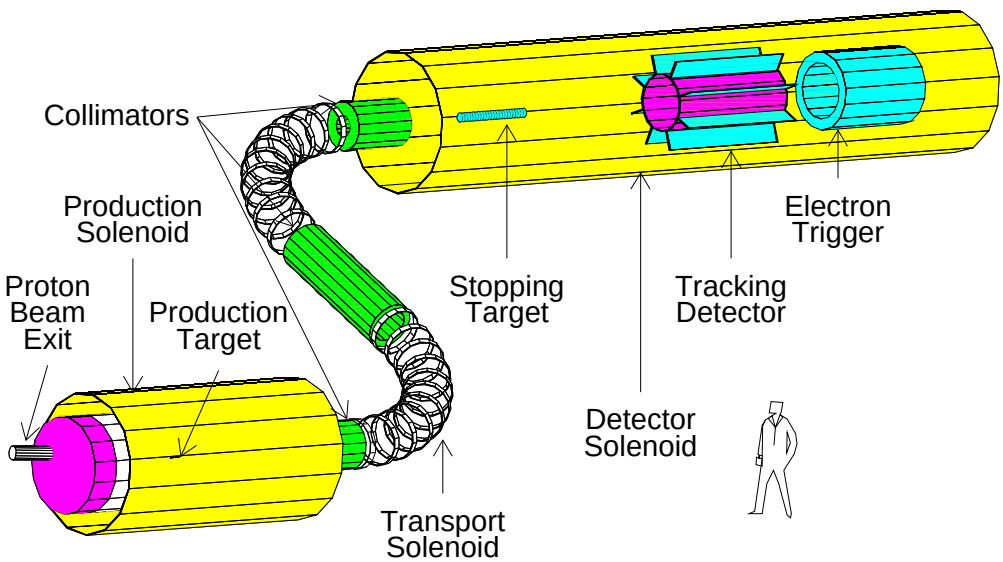

Fig. 5. Schematic drawing of the production solenoid, transport solenoid, and detector solenoid with the targets, collimators, and detectors.

The heart of the detector is the magnetic spectrometer in which the e^- momentum is measured. The tracking detector is low mass in order to minimize the contributions of multiple scattering and energy loss to the electron energy resolution. The electron trigger detector's primary purpose is to select events to be recorded for off-line analysis by requiring a deposited energy consistent with that of a 105 MeV electron. In addition, it provides some confirmation of the

e^- energy, aids in distinguishing e^- from other particles, and helps in identifying backgrounds from particles produced by cosmic rays. The detector region is surrounded by a cosmic ray shield, which minimizes the rate of production of electrons by cosmic ray muons and identifies the e^- that are produced by cosmic rays traversing the detector.

4.1 Physics Background Sources

Physics backgrounds potentially originate from a variety of sources: μ^- decay in a Coulomb bound orbit, radiative μ^- capture, beam electrons, μ^- decay in flight, π^- decay in flight, radiative π^- capture, $\overline{p}$ induced electrons, and cosmic ray induced electrons. The first two are intrinsic to μ^- stopped in the target; they can be minimized only by improving the measurement of the electron energy. The other sources derive from prompt processes, with the electron detected close in time to the arrival of a particle in the detector, and are reduced with a pulsed beam. Very slow $\overline{p}$'s have a very long transit time in the muon beam line and arrive at the stopping target essentially continuously. Hence, they are not significantly reduced by using a pulsed beam. Cosmic ray background is reduced with appropriate active and passive shielding.

Most of the potential sources of backgrounds were studied extensively by the MECO Collaboration. Particle production, decay, and interaction in the beam and detector were simulated using the GEANT code package. The simulation included effects of scattering in the beam line and collimators, inhomogeneities in the magnetic field in the transport region, and energy loss throughout the beam line. Some processes which are not well modeled by GEANT were calculated with a combination of analytic and Monte Carlo techniques. For example, large angle scattering of electrons in the stopping target was simulated using the Mott scattering formula with nuclear form factors. Rates for some processes (radiative π^- and μ^- capture, for example) have been taken from the literature and incorporated in a Monte Carlo calculation of the background. In the following, the number of background events reported corresponds to an experimental sensitivity of five signal events for $\mathrm{R}_{\mu e} = 10^{-16}$.

The intrinsic background from μ^- decay in orbit is approximately proportional to $(E_{max} - E_e)^5$ near the endpoint.[23] Hence, it is extremely sensitive to both the central part of the detector response function and possible high energy tails.

Figure 6 shows the signal and background for $R_{\mu e} = 10^{-16}$, calculated in a full GEANT simulation.[24] By accepting events between 103.9 MeV and 105.4 MeV, the noise to signal ratio is below 0.05 and the signal acceptance is large.

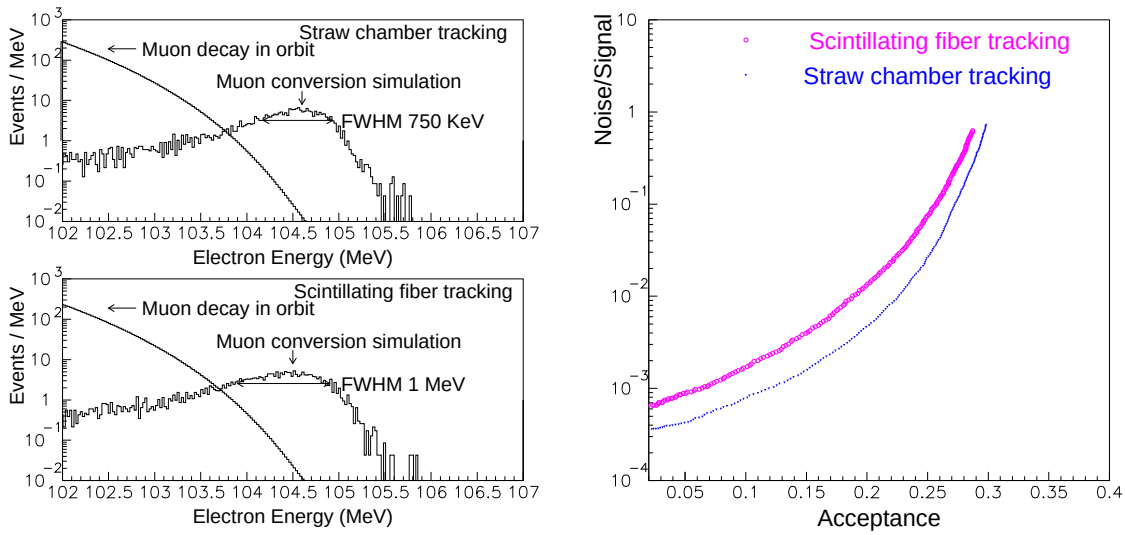

Fig. 6. The histograms on the left show simulations of the expected signal and background for $R_{\mu e} = 10^{-16}$ for two detectors. The normalization of the curves is for $R_{\mu e} = 10^{-16}$ and a luminosity corresponding to 10^7 seconds running time. On the right is a parametric plot of the background/signal and acceptance as a function of the minimum allowed measured e^- energy.

The radiative μ^- capture background results from the process μ^- Al $\rightarrow \gamma\nu_\mu$ Mg. The photon endpoint energy is 102.5 MeV and the probability (per μ^- capture) of producing a photon with energy exceeding 100.5 MeV is $\sim 4 \times 10^{-9}$ (Ref. 25). The γ conversion probability in the target is ~ 0.005, and the probability that the electron energy exceeds 100 MeV is ~ 0.005. The probability of misreconstructing the energy by more than 1.9 MeV is less than 10^{-5}. The background from radiative μ capture is less than 0.05 events.

Beam electrons which cause background are produced in the production or transport solenoid region and then scatter in the stopping target, simulating signal events. The rate for electrons scattering at $\sim$ 100 MeV/c is defined by the Mott cross section modified by a nuclear form factor. The collimator system is designed to suppress high energy electrons. A GEANT simulation of the production of electrons and their transport to the detector solenoid yielded no transmitted

electrons above 100 MeV for 10^7 incident protons. The beam electron background inferred from this calculation is below 0.002 events.

Muon decay in flight can result in energetic electrons which can fake signal. The background from decays in the detector solenoid is below 0.007 events. Background from π^- decay was shown by GEANT simulation to be negligible.

Pions stopping in the target are immediately captured by a nucleus and about 2% of them result in the emission of a photon[26] without significant nuclear excitation. The γ energy spectrum has a peak at 110 MeV and endpoint at 140 MeV. The probability of γ conversion in the Al target with a conversion electron in a 1.5 MeV energy interval around 104 MeV is 3.5×10^{-5}. The yield of π's which pass the transport solenoid and stop in the target is $\sim 6 \times 10^{-7}$ per proton. Accounting for the beam extinction of 10^{-10}, the background is 0.007 events.

Pions that take a very long time to traverse the production and transport solenoid can produce background, the level of which is more difficult to calculate. The suppression factor of 10^{-10} from the beam extinction is absent and this background is suppressed primarily by the small probability that a π^- survives the long transport time. By GEANT simulation it was found that this background is below 0.002 if the detection time starts 0.7 μs after the beam pulse.

Cosmic ray induced electrons are potentially a limiting background and were studied using a GEANT simulation[27] of the detector and shielding. This background can be reduced to a level of ~ 0.0035 events per 10^7 seconds of running time with a combination of active and passive shielding and by eliminating events in which extra particles are detected in the tracking detector.

Possible background from $\overline{p}$ in the beam is being studied actively by the MECO Collaboration. The $\overline{p}$ yield at low energy is not measured, and depends sensitively on the Fermi momentum in the nucleus. Several means to suppress this source of background exist, if it proves to be a problem. One is to simply lower the proton beam energy, which results in substantial reduction in $\overline{p}$ flux as one goes below a nominal $\overline{p}$ production threshold of 6.3 GeV. A second is to place thin absorbers in the muon transport channel. These can fully absorb the $\overline{p}$'s with little loss in muon flux, and the effect of the annihilation products is being studied. A third is to sweep the $\overline{p}$'s into a collimator in a crossed electric and magnetic field; an electric field of 2 MV/m in the 2 T transport field would be sufficient.

4.2 Detector Rates

Increasing the experimental sensitivity by a factor of 10^4 over current efforts requires much higher stopping rates ($\sim 10^{11}$ s^{-1}) and correspondingly higher detector rates. Rates in the SINDRUM2 detector are in fact very low.[28] The MECO design has improved geometry to further reduce rates. In particular, the detector is located about 2 m from the stopping target. This reduces the solid angle subtended by the detector and allows for the use of thin absorbers to reduce the flux of low energy protons hitting the detectors. Nonetheless, the very high muon stopping rate presents a challenge for the rate handling capabilities of the MECO apparatus. The detector gains will be reduced during the stopping pulse when rates are very high. During the detection interval, rates are dominated by p's and γ's from μ capture processes and e^- from μ^- decay in orbit. A full GEANT simulation of the detector was used to calculate MECO detector rates.

Approximately 10^{-4} of all e^- from μ^- decay in orbit have energy above 60 MeV, and the inner radius of the tracking detector was chosen to ensure that e^- with transverse momentum (p_t) below 60 MeV/c do not hit it. The average rate per detector element from this source is $\sim$ 48 kHz.

Every μ^- capture results in the production of excited nuclear states, radioactive nuclei, and/or neutron emission with the possibility of subsequent neutron-induced nuclear gamma rays. The approximate rate is two γ's per μ^- capture. The detector rate from γ's is dominated by conversion and Compton scattering of low energy (below 10 MeV) photons and is $\sim$ 70 kHz per detector element.

Neutrons are produced copiously following μ^- capture.[29] A GEANT simulation of the interaction of these neutrons in the detectors shows they contribute negligibly to the total rate.

Protons are also emitted following μ^- capture. The proton spectrum has been measured[30] using μ's stopping in emulsion, and is mostly below 15 MeV. The total flux of protons exiting the stopped target is large, with an instantaneous intensity exceeding 10^9 s^{-1}. The detector rate due to protons is reduced with a set of thin absorbers which attenuate the proton flux striking the detectors without substantially degrading the electron energy measurement. The resulting rate is $\sim$ 170 kHz per detector element.

The total rate per detector element is $<$ 300 kHz. To set the scale of the ability to do high precision tracking in these rate environments, this is lower by

a factor of 2–3 than rates in the BNL E871 straw chamber detectors of similar construction. In a 30 ns gate, typical of the drift time in straw detectors operated with a 100 μm/ns drift velocity gas, the average occupancy is under 1%.

Even though the expected rate is not large compared to current experiments, they are of concern, for example, due to the possibility of pattern recognition errors which could cause tails in the energy response function of the spectrometer. Most hits caused by protons and γ conversions can be distinguished by pulse height. The protons are low energy and heavily ionizing. Conversions of γ's result in low energy electrons which spiral in a few wires and also give large pulse height. The possibility of the high rate environment resulting in tails in resolution functions is being studied actively by the MECO Collaboration.

4.3 Pulsed Proton Beam

An appropriately pulsed beam is critical to background rejection in MECO. The experiment will use the rf structure of the AGS to produce a pulsed proton beam. The proposed operation of the AGS is with two filled bunches in the 2.7 μs revolution time, extracting the beam without de-bunching.[19] Resonant extraction gives a pulse width shorter than the filled bunch width and will result in narrow bunches separated by 1.35 μs.

The properties of a bunched extracted beam were measured.[31] One rf bunch was filled, accelerated to 24 GeV, and extracted. Figure 7 shows the relative

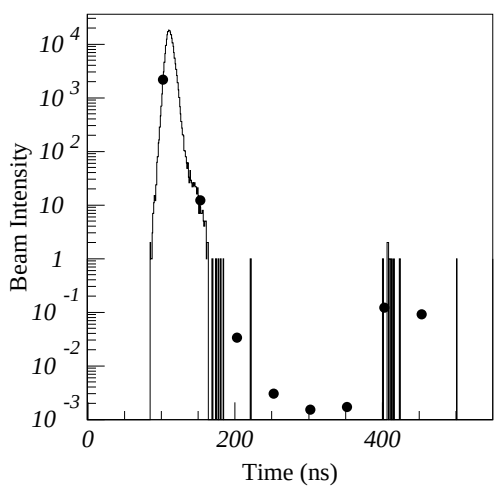

Fig. 7. Plot of the beam intensity as a function of time with respect to pulses in the bunched beam extracted from the AGS.

intensity as a function of time with respect to the filled bunch. The pulses are $\sim$ 15 ns wide and the extinction between bunches is below 10^{-6} and in unfilled bunches is of order 10^{-4}. These measurements were made with only minimal tuning of the AGS, and substantially improved performance is expected.[19]

It may not be possible to reach an extinction below 10^{-8} in the extracted beam, and other means of reducing the off pulse rate have been explored. The preferred solution is a pulsed kicker[32–34] in the proton transport line. The basic idea of the device is to produce a transverse deflection with a rectangular time structure by using a series of kickers, each driven sinusoidally; the amplitudes and phases on the individual kickers are adjusted to give a rectangular time structure. Both electrostatic and magnetic devices are being studied.

4.4 Muon Beam Design and Performance

The design of the μ^- production scheme is based on that of the MELC experiment[17,18] and adopted for the muon collider[20,21] source. Pions are produced in a tungsten target in a high field solenoid; those with sufficiently small transverse momentum travel in helical trajectories inside the solenoid and decay to μ's. The field is graded; the axial component varies from 3.3 T at the upstream end to 2 T at the muon beam channel entrance. Muons are transported to the stopping target with good efficiency in a curved solenoid[35] which also removes unwanted particles. It consists of a set of short solenoids arranged to form two bends, each of 90°, surrounded and separated by three straight sections, each containing a collimator. The arrangement is shown in Fig. 5.

Figure 8 shows a schematic drawing of the production solenoid and beginning of the transport solenoid, on which a typical event is superimposed. The target is a radiation cooled, 0.8 cm diameter, 16 cm long tungsten cylinder. The superconducting coil is protected with a heat and radiation shield made of tungsten and copper with an inner radius of 0.3 m. The proton beam enters through a hole in the downstream end of the solenoid, and non-interacting protons exit through a larger hole in the upstream end. The direction of the proton beam is opposite that of the muon beam in order to simplify construction of the exit channel and the heat shield, and to minimize the fluence of γ's, neutrons, and $\overline{p}$'s entering the transport solenoid. Low energy pions are produced at all angles, and the use of a

graded field minimizes the loss of pion yield resulting from targeting the protons in the backward direction.

With an incident flux of 2×10^{13} protons per second, the maximum target temperature is below 2,450 K (Ref. 36). At this temperature the target would lose 0.1% of its mass in a one-year run due to evaporation. Incident fluxes a factor of two higher would result in significantly increased evaporation rates, and means of reducing the heat load with different target shapes are being explored. Heat load from the particle spray on the super-conducting solenoid surrounding the production target is manageable based on results of a GEANT calculation.[37] Less than 50 W is deposited in a 6 cm thick coil pack outside the shield. The maximum instantaneous local heat load is below 0.2 mW/gm and the total radiation load in a 10^7 s run is below 50 Mrad.

There is little precise information on low energy pions produced by protons of a few GeV/c incident on heavy targets. These production cross sections are

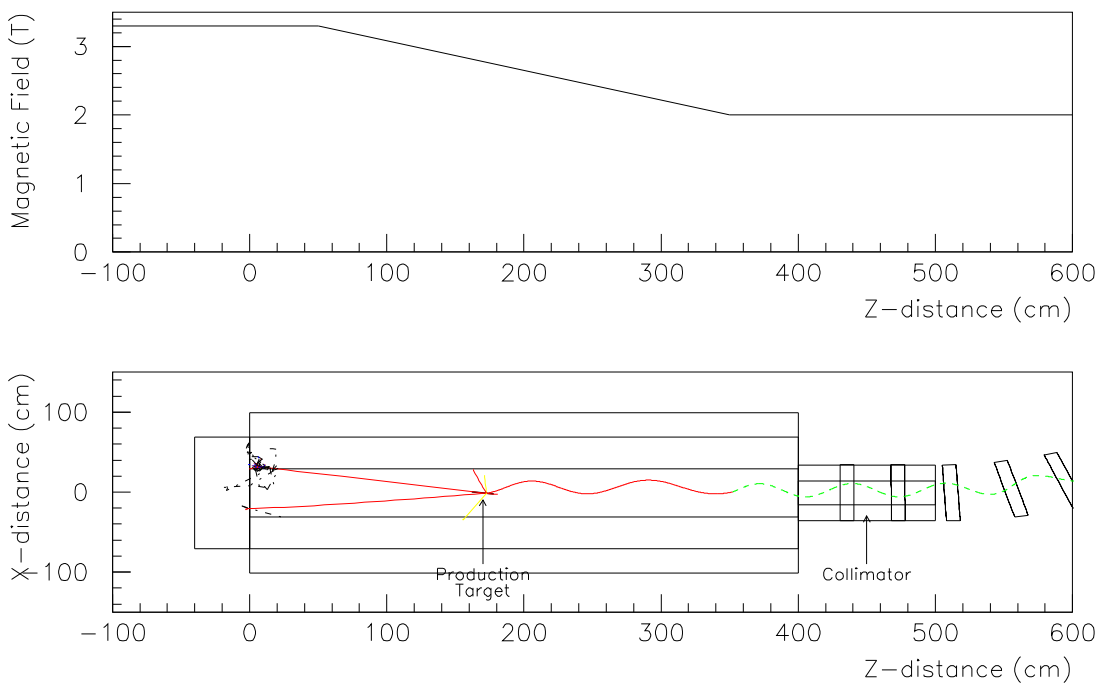

Fig. 8. Schematic drawing of the production solenoid, on which a simulated event with a proton interaction is superimposed, producing a μ^-. The incident proton beam enters from the right. Above the drawing is a plot of the axial component of the magnetic field in this region as a function of z.

now being measured by E910 (Ref. 38) at BNL. Model calculations based on FLUKA,[39] GHEISHA,[40] SHIELD,[41] MARS,[42] DPMJET2,[43] and ARC[44] vary by a factor of six. The production and transport parameters were optimized,[45,46] and the resulting pion yield calculated using the GHEISHA code in the GEANT simulation package. Subsequent to those calculations, the results of which are contained in the MECO proposal, a measurement[47] of low energy pion production by 10 GeV protons on heavy targets was found which indicates[48] the GHEISHA model overestimates the yield by about a factor of two.

Charged particles are transported to the detector solenoid using a curved solenoid, one purpose of which is to decrease the transmission of both high momentum and positive particles. Charged particles of sufficiently low momentum follow helical trajectories centered on magnetic field lines. In a torus, they drift in a direction perpendicular to the plane of the torus, by an amount given by $D = 1/0.3\ B \times s/R \times (p_s^2 + \frac{1}{2}p_t^2)/p_s$, where D is the drift distance, B is the magnetic field, s/R is the bend angle of the solenoid, and p_t and p_s are the perpendicular and parallel momentum components. For $s/R = \pi/2,\ p_t = 0.09$ GeV/c, $p_s = 0.12$ GeV/c, and $B = 2$ T, the drift of the center of the helix is 49 cm. The drift direction depends on the charge. The drift effect is illustrated in Fig. 9. Collimators which remove most positive particles and all negative particles above 100 MeV/c are placed in the straight sections (shown in Fig. 9). The results of the calculations of muon yields are discussed in the section on expected MECO sensitivity.

4.5 The Stopping Target and Tracking Detector

The stopping target and detectors are located in a solenoid of radius ~ 0.9 m, with a graded axial field, varying from 2 T at the entrance to 1 T in the region of the detectors. The use of a graded field has two consequences. First, the quantity p_T^2/B_Z is constant, and hence 105 MeV e^-, either in the beam or produced at the upstream end of the solenoid, will have $\mathrm{p}_T < 74$ MeV/c at the detector and can be eliminated as background by requiring $\mathrm{p}_T > 75$ MeV/c. Second, conversion electrons emitted at angles of $90° \pm 30°$ with respect to the solenoid axis will have trajectories which intercept the tracking detector and which have a restricted range of p_T. Those initially moving away from the detector bounce in the graded field. This allows the tracking detector to be in a uniform field region,

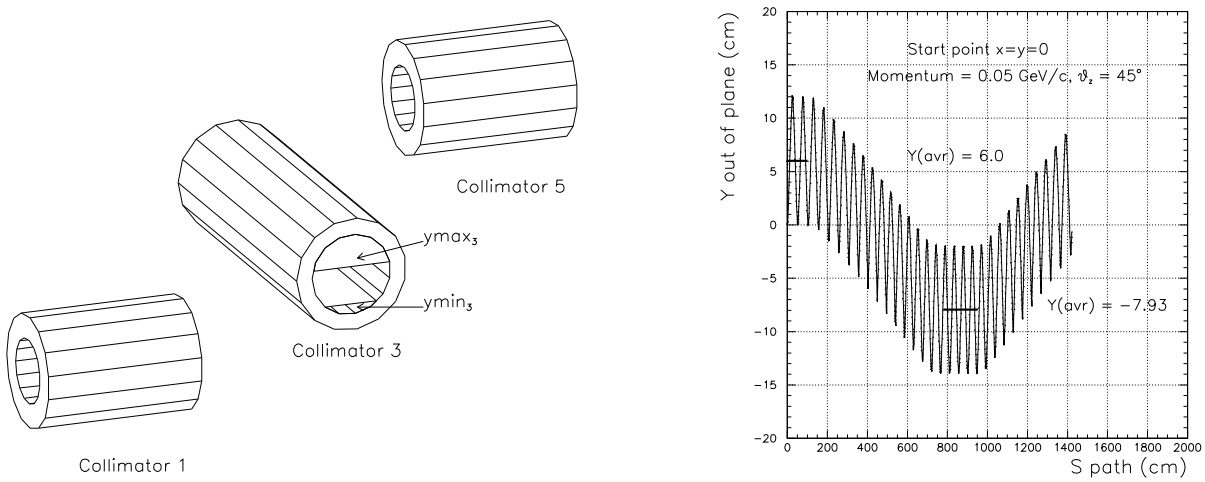

Fig. 9. The arrangement of the collimators that are used to eliminate high energy negative and all positive particles from the beam is shown on the left. On the right is a plot of the drift of a particle perpendicular to the plane of the transport as a function of the total path-length. It drifts down in the first half of the transport solenoid and back up in the second half.

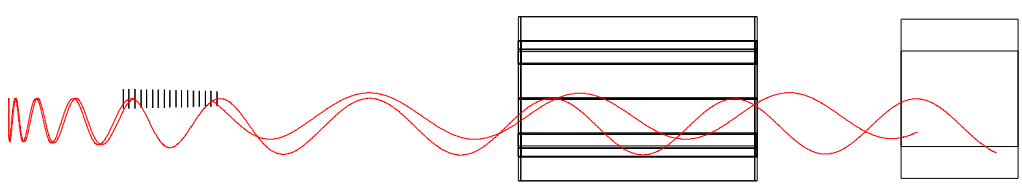

Fig. 10. A schematic drawing of the MECO detector region with two typical conversion electron trajectories produced by the GEANT simulation superimposed.

and displaced from the stopping target, which minimizes rates in the detector. Sample trajectories illustrating this are shown in Fig. 10.

The goal for the tracking detector is to measure with good efficiency the parameters of the helical trajectory of electrons. The uncertainty in the measurement is dominated by multiple scattering. The detector consists of a cylinder and eight equally spaced *vanes* of tracking detectors, as shown in Fig. 5. All individual detector elements are oriented in the axial direction.

The baseline design of the cylinder and vanes uses three layers of 5 mm diameter, 2 m long straw tubes. The axial coordinate is measured using pads external to the straws, in which signals are induced. The straws will be made of carbon loaded kapton. An alternate design has been studied in which the cylinder consists of four layers of 0.5 mm diameter scintillating fibers, arranged in pairs at small angle stereo, to get the axial coordinate.[49] This design is easier to manufacture, but there is more scattering and energy loss in the cylinder, which reduces the precision of the electron energy measurement.

The performance of the detectors was calculated using a full GEANT simulation of the stopping target and detectors.[24] It incorporated the Moliere scattering formalism and Landau fluctuations in the energy loss. It used Gaussian measurement errors with σ_x, σ_y, and σ_z equal to 0.2 mm, 0.2 mm, and 1.4 mm, respectively. This spatial resolution is easily achieved in both technologies. Figure 10 shows a few typical events in the simulation.

To ensure that the events have well-measured trajectories, only events with at least three hit segments in a single turn and four total hit segments are used. A trajectory which goes through all hit segments is calculated using a maximum likelihood method. It determines the trajectory connecting each pair of hit segments as a function of the electron momentum, p_e, and then minimizes the likelihood, $L(p_e)$, as a function of p_e. $L(p_e)$ is simply the product of the scattering probability at each detector position. The uncertainty in the fit is derived from the shape of the likelihood function in the region of the peak. The σ_{RMS} is 170 and 240 keV, respectively, for the straw and fiber detectors; this is increased to a FWHM of 750 and 1,000 keV, respectively, with a low energy tail, when the effect of energy loss straggling in the stopping target is included. To select signal events, suitable requirements on the fitting quality were applied and the electron energy and p_T were required to exceed 103.9 MeV and 75 MeV/c. From these simulations, the

acceptance of the detector and analysis scheme was determined; this is discussed in the section on the expected sensitivity of MECO.

Using the resolution function determined from Monte Carlo simulated events, the level of muon decay in orbit background was calculated[24] by convolving the resolution function and the background electron energy spectrum. Figure 6 shows the noise to signal ratio vs acceptance for the two detector possibilities, parameterized as a function of the lower edge of the accepted electron energy range. This and other background contributions are summarized in the section on the expected sensitivity of MECO.

4.6 Electron Trigger Calorimeter

The purpose of the electron trigger calorimeter in the MECO experiment is to detect electrons with $\sim$ 105 MeV energy that have passed through the tracking system. The proposed detector[50] is a scintillator cylinder of outer radius 70 cm, inner radius 41 cm, and 1 m in length. For the purpose of determining the position and arrival time of electrons at the detector and minimizing the effects of pileup on the energy measurement, the device is divided into 32 azimuthal by 50 axial segments. It is read out by WLS fiber. A schematic drawing of the device is shown as the insert in Fig. 11.

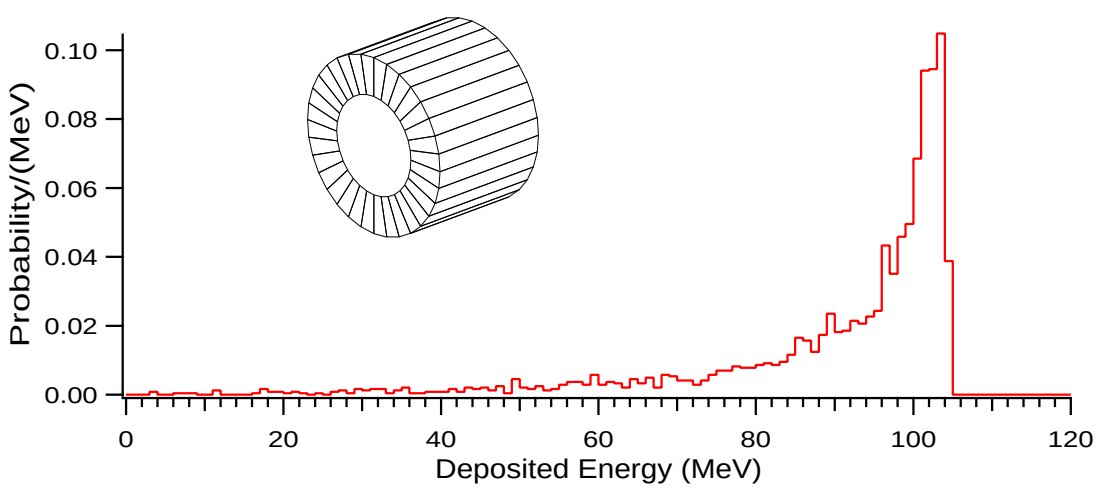

Fig. 11. The energy response of the electron trigger calorimeter for 105 MeV electrons. The inset shows the geometry of the detector. Each azimuthal slice is divided into $\sim$ 50 tiles.

The performance was studied with a GEANT simulation. The distribution in the energy deposited by 105 MeV conversion electrons is shown in Fig. 11. The low energy tail is due to electrons that are near the transverse acceptance limit of the tracker. This resolution function will be broadened by pileup. Protons resulting from muon capture are low energy, can be fully absorbed in a very thin shell surrounding the calorimeter, and will not deposit energy into it. There will be additional energy deposited into the calorimeter by neutrons and γ's from the stopping target. The average energy deposited in two wedges in a 50 ns time window is $\sim$ 5 MeV with an RMS dispersion of $\sim$ 3 MeV.

The trigger rate will be dominated by the high energy tail of e^- from muon decay in orbit. It has been estimated by convolving the electron energy distribution with the response function of the calorimeter and imposing a minimum energy requirement of 65 MeV. Without the effects of pileup of photons and neutrons, the trigger rate is $\sim$ 1.0 kHz. This increases to 1.3 kHz with the nominal flux of photons and neutrons, and to 1.7 kHz if the flux is assumed to be twice the expected level. Hence, a simple, single level trigger selecting only on energy deposited in the calorimeter will result in very low trigger rates.

4.7 Cosmic Ray Shielding

A potential source of background is cosmic ray induced electrons. This source is unique in that the number of background events is proportional to the data collection time, and not to the sensitivity. Further, improved energy resolution reduces the background, since electrons from cosmic rays will be distributed uniformly in energy in the region of interest. Hence, significant improvement (with respect to that of earlier experiments) in CR induced background rejection is not required. Placing the detector in a graded solenoidal field also provides benefits in reducing background. Most importantly, there is a restricted range of p_T for electrons produced in the stopping target and detected in the spectrometer.

The background is reduced with a combination of active and passive shielding. It consists of 0.5 m of steel (some of which is provided by the return yoke of the magnet) surrounding the detector solenoid, two layers of plastic scintillator, and 2 m of concrete shielding. It is assumed that the probability of not detecting a penetrating charged particle in either layer of scintillator is 10^{-4}. The scintillator veto shield contains $\sim$ 300 m^2 of scintillator; one possible implementation is to

use an extruded plastic scintillator similar to that now intended to be used in the MINOS neutrino detector.

The cosmic ray induced background was calculated using measured cosmic ray μ^- fluxes[51] and a GEANT simulation of the shielding and detector.[27] Muons dominate the flux of particles penetrating any significant amount of shielding. The rate of background induced by cosmic rays in which no charged particle traverses the active veto is very small. The calculation accounts for electrons produced by muons penetrating the shielding and decaying in the detector solenoid or interacting in the target and detectors. Particles were eliminated as potential background based on selection criteria including the measured momentum, p_T, charge, projection to the muon stopping target, fitting quality, number of detector elements with signals expected but missing, and energy deposited in the electron trigger detector.

In a simulation equivalent to $\sim$ 200 years exposure, three events satisfied all selection criteria; they are shown in Fig. 12. From this simulation, the cosmic ray background is predicted to be 0.0035 events in 10^7 seconds of exposure.

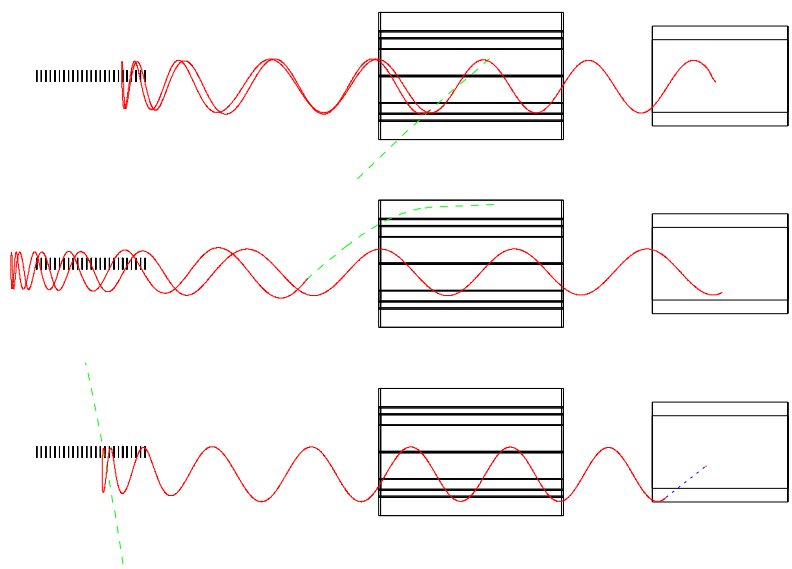

Fig. 12. Sample CR induced background events: a δ-ray produced in the straw material, a μ decay, and a δ-ray produced in the stopping target.

4.8 Expected Performance and Sensitivity of MECO

The sensitivity which will be achieved by MECO depends on the running time, proton intensity, number of muons per proton produced and transported to the stopping target, stopping probability, fraction of stops which capture (as opposed to decay), trigger efficiency, accidental cosmic ray veto loss, tracking acceptance, and losses due to analysis inefficiencies and background rejection selection criteria. The values of the acceptance and efficiency for these are given in Table 2. Loss of events due to accidental cosmic ray vetos and dead-time losses are expected to

Table 2. A summary of the expected MECO sensitivity for a one-year (10^7 s) run.

Running time (sec)	10^7
Proton flux (sec^{-1})	4×10^{13}
μ/p entering solenoid	0.006
Stopping probability	0.370
μ capture probability	0.600
Fraction of μ which capture in time window	0.480
Electron trigger efficiency	0.900
Fitting and selection criteria	0.250
Detected events for $R_{\mu e} = 10^{-16}$	5.800

be small; losses in pattern recognition in the tracking detector are also expected to be small but have not yet been estimated. In one year (10^7 s) running time, a few events can be detected at a value of $R_{\mu e} = 10^{-16}$.

The muon yield used in Table 2 is different from that in the MECO proposal. We have updated the number based on the measurements of pion yields discussed earlier, which gives a muon flux a factor of two lower than the GHEISHA prediction. The proton intensity has been increased with respect to that reported in the proposal by a factor of two based on the new expectation for AGS cycle time when running the machine at 8 GeV. If it is necessary to reduce the proton energy to 5 GeV to eliminate backgrounds from $\overline{p}$'s, the muon yield will decrease by a factor of two, resulting in ~ 3 detected events for a branching fraction of 10^{-16} in

a 10^7 second run. The experiment is not limited by backgrounds, and increased running time will improve the sensitivity proportionally.

Table 3 shows the expected background rates for the sensitivity quoted above. The background is dominated by the μ^- decay in orbit contribution. Substantial

Table 3. A summary of the level of background from various sources, calculated for the sensitivity given in the previous table, and with scaling as discussed in the text.

Source	Events	Comment
μ decay in orbit	0.29	signal/noise = 20 for $R_{\mu e} = 10^{-16}$
Radiative μ capture	$<< 0.05$	
μ decay in flight	< 0.003	without scatter in target
μ decay in flight	0.004	with scatter in target
Radiative π capture	0.007	from proton during detection time
Radiative π capture	0.014	from late arriving π
π decay in flight	$<< 0.001$	
Beam electrons	< 0.002	
Cosmic ray induced	0.004	assuming 10^{-4} CR veto inefficiency
Total background	0.37	

improvement in discrimination against this source of background can be had with modest loss in acceptance, as shown in Fig. 6. For example, the background/signal ratio can be decreased from 0.05 to 0.02 with a relative loss in sensitivity of less than 10%.

Many of the backgrounds depend on the proton beam extinction. We explicitly assume that the number of protons hitting the production target during a time corresponding to the detection time is less than 1 for 10^{10} protons hitting the target during the beam pulses. This beam extinction has not been demonstrated, and is being studied actively. The potential background due to $\overline{p}$'s in the beam has not yet been reliably estimated and is currently under study. At the proposed level, the experiment is not expected to be limited by background.

5 Summary

Experiments to search for violation of muon and electron number have now been done for over 40 years, with ever increasing sensitivity. Current limits on muon-induced processes are at the level of 10^{-11} to 10^{-12} for the processes $\mu^+ \to e^+\gamma$, $\mu^+ \to e^+e^+e^-$, and $\mu^- N \to e^- N$. These limits place stringent constraints on many scenarios for physics beyond the Standard Model.

Improvements in muon beams and detector technology hold promise for making further significant improvements in the sensitivity of searches in the next few years. In particular, the SINDRUM2 experiment being done at the PSI laboratory is expected to improve the sensitivity to $\mu^- N \to e^- N$ to below 10^{-13} in the next year or two. Further improvement, to a sensitivity below 10^{-16}, is promised by the MECO experiment, now approved at BNL. Ideas have been discussed for improving the sensitivity to $\mu^+ \to e^+\gamma$ to near 10^{-14}. If these proposed experiments are successfully executed, they will be sensitive to the level of lepton flavor violating signals suggested in many models. In particular, predictions of a class of grand unified supersymmetric models will be confronted directly by experimental measurements. The very substantial expected improvement in experimental sensitivity, coupled with the predictions of grand unified supersymmetric models, allow some optimism that the first evidence for muon and electron number violation may be found.

References

[1] R. Cahn and H. Harari *et al.*, Nucl. Phys. B **176**, 135 (1980).

[2] K. Arisaka *et al.*, Phys. Rev. Lett. **70**, 1049 (1993).

[3] T. Akagi *et al.*, Phys. Rev. Lett. **67**, 2614 (1991).

[4] P. Krolak *et al.*, Phys. Lett. B **320**, 407 (1994).

[5] A. M. Lee *et al.*, Phys. Rev. Lett. **64**, 165 (1990).

[6] U. Bellgardt *et al.*, Nucl. Phys. B **299**, 1 (1988).

[7] M. D. Cooper *et al.*, in *Proceedings of the Sixth Conference on the Intersections of Particle and Nuclear Physics*, edited by T. W. Donnelly (AIP Conference Proceedings 412, 1997), pp. 34–48.

[8] F. Riepenhausen, presented at the *Sixth Conference on the Intersections of Particle and Nuclear Physics*, Big Sky, Montana (1997).

[9] W. Marciano, *Proceedings of the 4th KEK Topical Conference on Flavor Physics*, edited by Y. Kuno and M. Nojiri, Nucl. Phys. B **59** (1997).

[10] R. Barbieri *et al.*, "Violations of lepton flavor and CP in supersymmetric unified theories," IFUP-TH 72/94, January 1995; R. Barbieri, L. Hall, and A. Strumia, Nucl. Phys. B **445**, 219 (1995).

[11] N. Arkani-Hamed *et al.*, "Flavor mixing signals for realistic supersymmetric unification," LBL-37343 (1996).

[12] R. Barbieri and L. Hall, "A grand unified supersymmetric theory of flavor," LBL-38381 (1996).

[13] J. Hisano *et al.*, "Exact event rates of lepton flavor violating processes in supersymmetric SU(5) model," LBL-38653 (1996).

[14] Y. Kuno and Y. Okada, LANL hep-ph/9604296 (1996); Y. Kuno, A. Maki, and Y. Okada, LANL hep-ph/9609307 (1996); C. Walter, private communication.

[15] A. Czarnecki, W. Marciano, and K. Melnikov, hep-ph/9801218 (1997).

[16] M. Bachman *et al.*, "A search for $\mu^- N \to e^- N$ with sensitivity below 10^{-16}," AGS P940 (1997).

[17] R. M. Djilkibaev and V. M. Lobashev, Sov. J. Nucl. Phys. **49(2)**, 384 (1989).

[18] V. S. Abadjev *et al.*, "MELC experiment to search for the $\mu^- A \to e^- A$ process," INR preprint 786/92, November 1992.

[19] M. Brennan, private communication.

[20] "Beam Dynamics and Technology Issues for $\mu^+\mu^-$ Colliders," edited by J. Gallardo (1995).

[21] "$\mu^+\mu^-$ Collider, a Feasibility Study," the $\mu^+\mu^-$ Collaboration, edited by J. Gallardo (1996).

[22] A. Badertscher *et al.*, Nucl. Phys. A **377**, 406 (1979).

[23] O. Shankar, Phys. Rev. D **25**, 1847 (1982).

[24] T. J. Liu, meco-004, "Initial resolution studies" (1997)
(see http://meco.ps.uci.edu for more information about MECO technical memos).

[25] A. Frischknecht *et al.*, Phys. Rev. C **2**, 1506 (1985).

[26] R. A. Eramzhyan *et al.*, Nucl. Phys. A **290**, 294 (1977).

[27] M. Overlin and W. Molzon, meco-014, "Estimates of cosmic ray induced background for MECO" (1997).

[28] A. van der Schaaf, private communication.

[29] T. Kozlowski *et al.*, Nucl. Phys. A **436**, 717 (1985).

[30] V. Balashov and R. Eramzhyan, "Muon capture by nuclei and problems of weak interactions," Atomic Energy Reviews **5**, (1967); H. Morinaga and W. Fry, Nuovo Cimento **10**, 308 (1953); C. Ishi, Prog. Th. Phys. **21**, 663 (1959).

[31] R. Lee, meco-017, "Timing measurements of AGS bunched beam extraction" (1996).

[32] W. Molzon, meco-006, "A pulsed electrostatic kicker for secondary extinction" (1997).

[33] A. Soukas, private communication.

[34] A. Soukas, J. Sandberg, and W. Meng, "A pulsed kicker for secondary extinction in a proton beam," BNL AGS memo (1997).

[35] W. Molzon, meco-008, "Schematic of transport solenoid based on Russian SC cable" (1997).

[36] R. Djilkibaev, meco-010, "Proton target temperature simulation" (1997).

[37] D. Garcia and W. Molzon, meco-018 "A study of heat loads on the MECO production solenoid" (1997).

[38] I. Chemakin *et al.*, P910 to BNL AGS (1995).

[39] P. A. Aarnio *et al.*, CERN/TIS-RP/190 (1987).

[40] H. C. Fesefeldt, "Simulation of hadronic showers, physics and applications," PYTHIA Report, Aachen 85-02 (1985).

[41] V. S. Barashenkov, N. M. Sololevsky, and V. D. Toneev, Atomn. Energ. **32** (1972).

[42] N. Mokhov, "The MARS code system user's guide," FNAL-FN-628 (1995).

[43] J. Ranft, "The DPMJET code system" (1995).

[44] Y. Pang *et al.*, Nucl. Phys. A **544**, 435 (1992).

[45] R. Djilkibaev, meco-009, "Pion yield and muon flux simulation" (1997).

[46] M. Bachman and R. Lim, meco-016, "Study of muon yields in MECO" (1997).

[47] D. Artmutliski *et al.*, Sov. J. Nucl. Phys. **48**, 161 (1988).

[48] R. Djilkibaev, meco-023, "MECO muon yield simulation using experimental data" (1997).

[49] D. Koltick, meco-020, "Light yield from a scintillating fiber tracker" (1997).

[50] S. Carabello and D. Koltick, meco-015, "Scintillating tile calorimeter for MECO" (1997).

[51] O. Allkofer *et al.*, Nucl. Phys. B **259**, 1 (1971).